Modulation and Soft-Switching Optimization Control of Multilevel Dual Active Bridge DC–DC Converters

Jupeng Pang, *Student Member, IEEE*, Kui Wang, *Senior Member, IEEE*, Mingzhe Wu, *Member, IEEE*, Wei Zhou, *Student Member, IEEE*, Zedong Zheng, *Senior Member, IEEE*, and Yongdong Li, *Senior Member, IEEE*

***Abstract*—The dual active bridge (DAB) converter has been recognized as one of the most promising dc–dc topologies. By introducing the multilevel structure, the DAB converter can be applied in dc distribution system of medium-voltage. In addition, the multilevel DAB (ML-DAB) converter has more freedoms to control the power flow and optimize its operating performance, for example, soft-switching performance. However, most of the existing researches only focus on the control and optimization of three-level DAB, due to the explosively-growing complexity as the number of voltage levels rises. Thus, complexity of control and optimization for ML-DAB restricts the practical implementation and application compared with conventional two-level (2L) DAB, which can achieve power flow control and operating performance optimization with only three phase-shifting ratios. Hence, to improve the performance of ML-DAB within feasible complexity, the quasi-two-level (Q2L) modulation and multiphase-shifting (MPS) control suitable for arbitrary *n*L-DAB are proposed in this article. The characteristics of power flow, inductor current, and soft switching for ML-DAB is analyzed by migrating the characteristics of 2L-DAB properly. Furthermore, an optimization control strategy to achieve full-range soft switching is proposed for ML-DAB. Compared with the existing *n*L modulation method for ML-DAB, the proposed Q2L modulation and MPS control methods can realize low-complexity control and high-performance operation of ML-DAB. Experimental results of a four-level DAB prototype are also presented for validation.**

***Index Terms*—DC–DC converter, dual active bridge, multiphase shifting, multilevel converter, soft-switching optimization.**

I. Introduction

With the rapid development of renewable energy, the dc power distribution system has been discussed extensively in recent years [1], [2]. The dc–dc converter, also named dc power electronic transformer that connects dc systems of different voltage levels, is one of the most essential equipment in dc power distribution systems.

Received 1 April 2024; revised 7 July 2024; accepted 14 August 2024. Date of publication 28 August 2024; date of current version 12 December 2024. This work was supported by Beijing Natural Science Foundation under Grant L242006. Recommended for publication by Associate Editor Giovanni De Carne. *(Corresponding author: Kui Wang.)*

Jupeng Pang, Kui Wang, Wei Zhou, Zedong Zheng, and Yongdong Li are with the State Key Laboratory of Power System, Department of Electrical Engineering, Tsinghua University, Beijing 100084, China (e-mail: pjp22@mails.tsinghua.edu.cn; wangkui@tsinghua.edu.cn; zw22@mails.tsinghua.edu.cn; zzd@tsinghua.edu.cn; liyd@tsinghua.edu.cn).

Mingzhe Wu is with the School of Mechanical and Electrical Engineering, China University of Mining and Technology-Beijing, Beijing 100083, China (e-mail: wmz@cumtb.edu.cn).

Color versions of one or more figures in this article are available at https://doi.org/10.1109/TPEL.2024.3450989.

Digital Object Identifier 10.1109/TPEL.2024.3450989

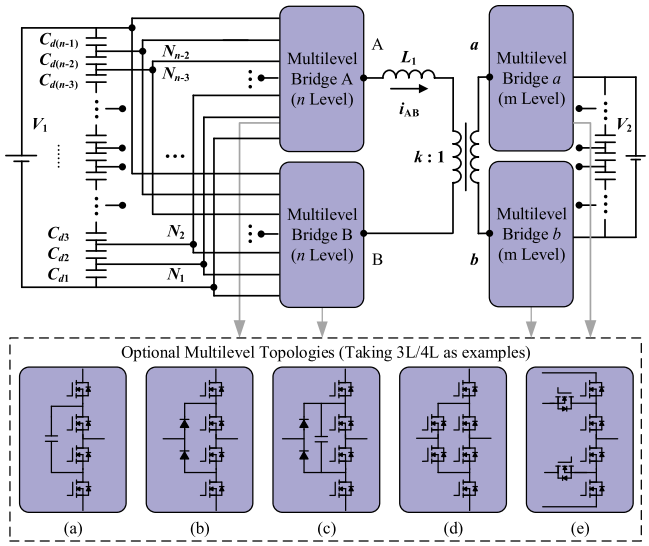

Fig. 1. Structure of ML-DAB with optional multilevel topologies (*n*L-*m*L DAB). (a) 3L-FC. (b) 3L-NPC. (c) 3L-HC. (d) 3L-ANPC. (e) 4L-ANPC.

Among various dc–dc converters, the dual active bridge (DAB) converter has gradually become one of the most promising topologies, which has the characteristics of bidirectional power flow, wide voltage conversion ratio, high efficiency, high power density, and galvanic isolation between primary and secondary sides [3]. Without the need for bulky industrial frequency transformer, DAB converters are widely used in space-limited scenarios, such as dc power distribution system of ships [2] and deep-sea dc power supply [4]. To meet the medium-voltage (MV) requirement of applications in dc distribution systems, the multilevel structure can be introduced in each side of DAB converters [5], which is the multilevel DAB (ML-DAB), as shown in Fig. 1.

Depending on whether the same number of voltage levels is adopted in primary and secondary sides, the ML-DAB can be classified into the symmetrical ($n = m$) and asymmetrical ($n \neq m$) structures. Up to now, both symmetrical and asymmetrical structures of the ML-DAB have been studied with various multilevel topologies, for example, the symmetrical three-level (3L) DAB (3L-3L DAB) converters with neutral-point clamped (NPC) [6], [7], active neutral-point clamped (ANPC) [8], hybrid-clamped (HC) [9], [10], [11], [12], [13] topologies, and the asymmetrical 3L two-level (2L) DAB (3L-2L DAB) converters with flying

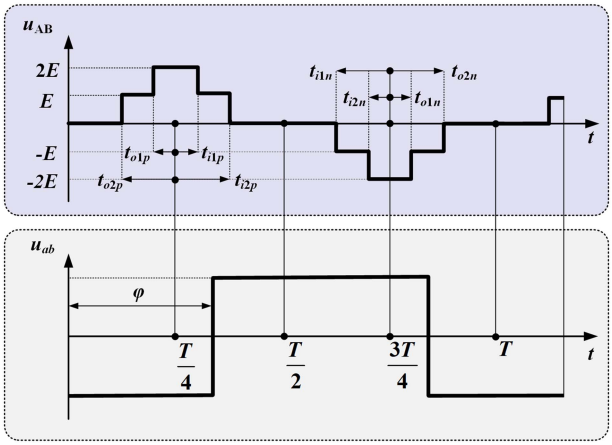

Fig. 2. Conventional 3L modulation for 3L-2L DAB.

TABLE I
COMPARISON OF THE COMPLEXITY OF NL-DAB

	the number of control variables	
SPS of 2L-DAB	1	
TPS of 2L-DAB	3	
3L modulation of 3L-2L DAB	Five for DAB control Five also for capacitor voltage balancing control	Complex coupling interaction
nL modulation of nL-2L DAB	**2n-1** for DAB control **2n-1** also for capacitor voltage balancing control	**Complex coupling interaction**
Proposed Q2L modulation and MPS control of nL-2L DAB	**Three** for DAB control **2n-4** for capacitor voltage balancing control	**Simple decoupling**

capacitor (FC) [14], NPC [15], [16], [17], ANPC [18], and HC [19] topologies.

By introducing the multilevel structure, the DAB converter can operate in MVdc applications with no use of input-series output-paralleled (ISOP) structure or less number of ISOP modules, thus, further increasing the power density. In addition, the introduction of multilevel structure can realize nL modulation for ML-DAB. On the one hand, the nL modulation can take full advantage of the low dv/dt and EMI of multilevel topologies, which is friendly to the design and operation of high-frequency transformers. On the other hand, the nL modulation offers extra degrees of freedom for the operating performance optimization of ML-DAB. The extra degrees of freedom offered by nL modulation in the ML-DAB case have same principles as the extra phase-shifting ratios offered by triple phase shifting (TPS) control in the 2L-DAB case, i.e., the voltage waveforms can be modified more flexibly through the extra degrees of freedom, and thus modifying the current waveform and instantaneous power to improve the operating performance of ML-DAB.

For the single phase shifting (SPS) and TPS control of 2L-DAB, the only phase-shifting ratio of SPS control is determined by the control of power flow with no possibility of other optimization control, while TPS control has more degrees of freedom for optimization control. The 3L (nL) modulation of ML-DAB is shown in Fig. 2, and the interval lengths of each voltage level can be adjusted as flexible degrees of freedom, with which the operating performance of ML-DAB can also be optimized when transferring appointed power flow, for example, the soft-switching performance [15], [20], [21], [10]. An optimal modulation for 3L-2L DAB converters based on equivalent-wave method is proposed to minimize current stress in [20]. Song et al. [15], [21] proposed a control strategy for 3L-2L DAB converters to achieve soft-switching and current stress optimizing based on analytic zero voltage switching (ZVS) constraints of ML-DAB. The soft-switching performance of 3L-3L DAB is analyzed in [10] and it gives a detailed theoretical ZVS operation range analysis varied with phase-shift angles and voltage conversion ratio.

However, despite the above extensive studies on operating performance optimization control of ML-DAB converters, most of them only involve the 3L case. And the existing nL modulation and control methods are difficult to be migrated to the case of 4L, 5L, or arbitrary nL, because the complexity of nL modulation increases explosively with the number of voltage levels. To provide a comparison of the complexity between 2L-DAB, 3L-DAB, and nL-DAB, the TPS control of 2L-DAB is chosen as a candidate, while the 3L (nL) modulation guaranteeing the odd symmetry and odd harmonic symmetry ($t_{\mathrm{o1p}} = t_{\mathrm{i1n}}$, $t_{\mathrm{o2p}} = t_{\mathrm{i2n}}$, $t_{\mathrm{i1p}} = t_{\mathrm{o1n}}$, $t_{\mathrm{i2p}} = t_{\mathrm{o2n}}$) shown in Fig. 2 is chosen to make sure the comparison is fair. As shown in Table I, considering the control of primary and secondary converters of DAB and the phase shifting between the two sides, it needs $2n$-1 variables to control the nL-DAB, which is consistent with the case of TPS control for 2L-DAB if $n = 2$. And the optimization control of 2L, 3L, and nL-DAB, for example, the soft-switching optimization, can be modeled similarly, so the number of variables for control can represent the complexity of control. Moreover, the balanced dc-link capacitor voltages are critical for the normal operation of ML-DAB, which also requires the complex balancing control strategy and relies on the above $2n$-1 variables for nL modulation.

Therefore, considering the higher number of variables to control and the presence of capacitor voltage balancing control, the ML-DAB is more complex than 2L-DAB when adopting the conventional nL modulation and control methods, and the complexity will increase explosively along with the increasing number of voltage levels and the coupling interaction between the DAB control and capacitor voltage balancing control. In a word, although the ML-DAB possesses more degrees of freedom to control than 2L-DAB, the conventional nL modulation and control method also makes it faced with much more complexity for practical control and implementation.

Hence, to mitigate the complexity of modulation, control, optimization, and implementation for ML-DAB, this article proposes a quasi-2-level (Q2L) modulation and multiphase shifting (MPS) control methods for ML-DAB. Based on the proposed Q2L modulation and MPS control methods, the characteristics of power flow, inductor current, and soft switching for ML-DAB can be analyzed and migrated from the characteristics of 2L-DAB. The main contributions of this article can be summarized as follows.

1) In dc–dc applications, the Q2L modulation is applied in multilevel modular dc–dc converter mostly, which adapts to control the bypass or switch-in of huge numbers of submodules. This article proposes the idea of utilizing the Q2L modulation in NPC-based ML-DAB dc–dc converters, aiming to ensure the quasi-identical characteristics of ML-DAB and 2L-DAB, which can greatly reduce the control complexity of ML-DAB. Moreover, the coupling interaction between Q2L and MPS control is clarified and solved in this article, rather than simple combination of them.
2) The proposed Q2L modulation and MPS control are appropriate for ML-DAB of arbitrary number of voltage levels. The introducing of inner phase-shifting between the converter legs for ML-DAB makes its control as simple as conventional 2L-DAB and the studies of 2L-DAB can be migrated to ML-DAB, which significantly facilitates the implementation and application of ML-DAB. Furthermore, it has constant control complexity for ML-DAB as the number of voltage levels increases.
3) The inductor current characteristics of ML-DAB is modeled precisely based on the current characteristics of conventional 2L-DAB, which does not require to conduct the complicated expressions of nL case. In addition, an optimization control strategy is introduced to achieve full-range soft switching across a wide range of voltage matching degrees between primary and secondary sides. Furthermore, the implementation processes are designed by integrating power flow (output voltage) closed-loop control with soft-switching optimization control.

Without the loss of generality, the asymmetrical multilevel structure ($m = 2$) is taken as an example in this article, and it is similar for the analysis of symmetrical cases because of the symmetry between primary and secondary sides.

The rest of this article is organized as follows. Section II presents the Q2L modulation and MPS control of ML-DAB converters. The soft-switching optimization control is elaborated on in Section III. Section IV presents the experimental verifications for proposed modulation and control methods and provides a comparison with the existing nL modulation method. Finally, Section V concludes this article.

II. Q2L Modulation and MPS Control of ML-DAB

For an n-level DAB converter, the primary dc-link comprises n-1 capacitors, as shown in Fig. 1. In its normal operation, the capacitor voltage should equally partition the dc-link voltage with each sharing $E = V_1/(n\text{-}1)$. It is noteworthy that the capacitor voltage balancing control is also a hotspot in the research of ML-DAB, and various capacitor voltage balancing methods are proposed based on conventional nL modulation method [22], [23]. Actually, the issue of capacitor voltage balancing control under proposed Q2L modulation was involved in the previous work of authors [24], in which a capacitor voltage balancing method by adjusting the dwell time of Q2L modulation was proposed for 4L-ANPC-DAB and it can also be extended to ML-DAB of any levels. Hence, in this article, the principle of Q2L modulation and the MPS control for power flow control and soft-switching performance optimization are emphatically focused, with the premise of capacitor voltage being well-balanced.

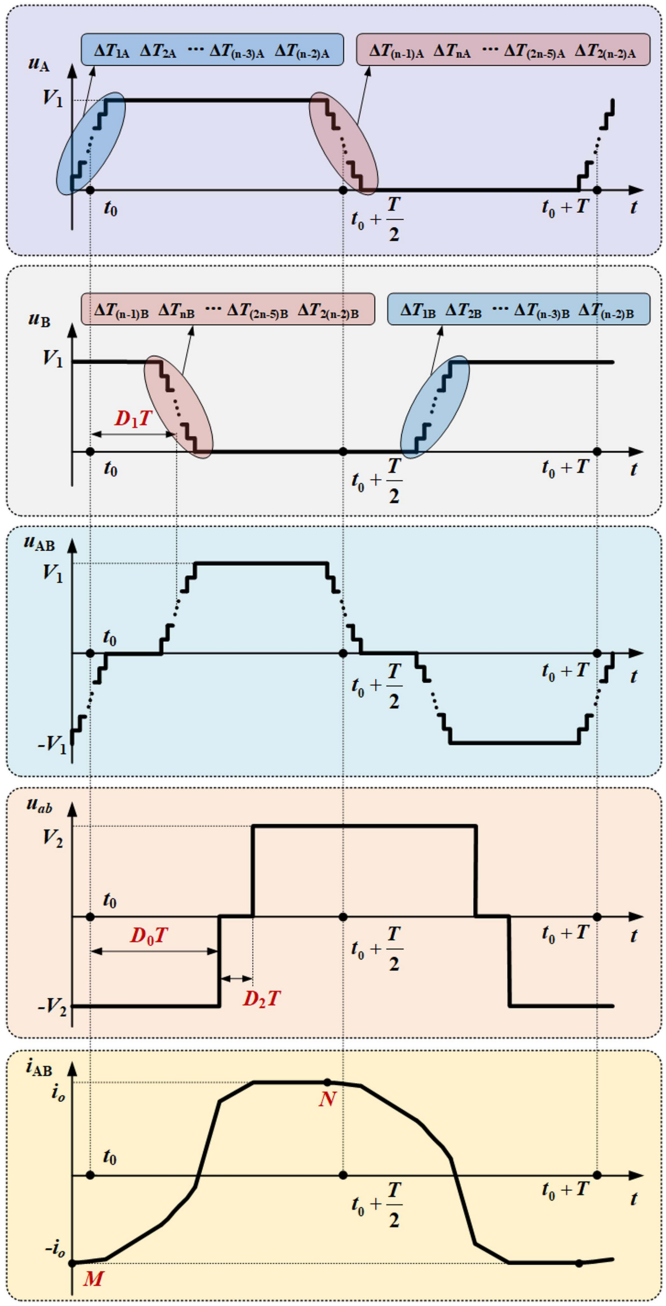

Fig. 3. Q2L operation and MPS control of ML-DAB. ($V_1 = kV_2$ as an example).

Fig. 3 illustrates the operating principle of Q2L modulation and MPS control. Here, T represents the switching cycle, while t_0, t_0+T/2 denote the onset and midpoint of a switching cycle, respectively. To be strictly located in the middle of the rising/falling edge, t_0, t_0+T/2 are determined based on the parity of n according to the following principles.

1) If n is even, t_0, t_0+T/2 are determined as the initial point of $\Delta T_{n/2}$, $\Delta T_{(3n\text{-}4)/2}$, respectively.

2) If n is odd, t_0, $t_0+T/2$ are determined as the midpoint of $\Delta T_{(n\text{-}1)/2}$, $\Delta T_{(3n\text{-}5)/2}$, respectively.

A. Q2L Modulation of Primary Multilevel Bridges

In Fig. 3, each multilevel bridge operates with Q2L modulation. For the modulation of an n-L half bridge, there will be 2(n-2) variables required to determine the Q2L waveforms, i.e., the dwell time for outputting the NP voltage denoted by ΔT_{ij}, ($i = 1,2,\ldots,2(n\text{-}2)$; $j =$ A, B), which is typically of small magnitude, such as hundreds of nanoseconds. Consequently, the voltage waveforms of the multilevel bridge closely resemble the 2-L square waveforms.

Considering the switching cycle and voltage levels, there exists both upper and lower limitations on ΔT_{ij}, as in (1). The upper limitation aims to sustain approximate square waveforms and ensure high power transfer capability. The lower limitation stems from the switching speed of device.

$$\begin{aligned} &\Delta T_{\min} \le \Delta T_{ij} \le \Delta T_{\max} \\ &(i = 1, 2, \cdots, 2(n-2)), j = A, B). \end{aligned} \tag{1}$$

Furthermore, to eliminate the dc component of transformer current and prevent saturation, the voltage-second product of u_{AB} within each switching cycle must equate to zero, which can be fulfilled by (2).

In summary, in the modulation of ML-DAB, the selection of suitable $\Delta T_{\min}$ and $\Delta T_{\max}$ should be conducted first. Then, the ΔT_{ij} satisfying (1), (2) shown at the bottom of this page, should be guaranteed along with the normal operation of the ML-DAB.

B. MPS Control of ML-DAB

In Fig. 3, the ML-DAB operates with MPS control, where D_0 is the outer phase-shifting ratio between the primary and secondary voltages, while D_1, D_2 represents the inner phase-shifting ratio of voltages of primary bridges and secondary bridges, respectively.

In practice, the proposed Q2L modulation and MPS control method mainly utilize three phase-shifting angles to control the power flow and optimize the operating performance of multilevel DAB. Although there exist 4(n-2) variables ΔT_{ij} for the Q2L modulation, the ΔT_{ij} can be set as a fixed value initially and easily adjusted under the capacitor voltage balancing control strategy proposed in [24] previously. For the little influence of the ΔT_{ij} and its adjustment on the power flow control, it can be neglected if ΔT_{ij} is far smaller than the phase shifting (D_0T, D_1T or D_2T). For larger ΔT_{ij} or more levels, the influence of ΔT_{ij} can be compensated through the slight adjustment of D_0, D_1, D_2 by closed-loop control.

Hence, the real implementation of the proposed modulation and control methods is not that complex due to the decoupling between the dwell time ΔT_{ij} adjustment (capacitor voltage balancing control) and the MPS control (power flow and operating performance control). And the proposed MPS control method of power flow and operating performance for ML-DAB has the same number of control variables as the conventional TPS for 2L-DAB and thus the complexity of such control remains constant as the number of voltage levels increases.

However, to obtain the analytical expression of voltages for the primary ML converter is much more challenging than the 2L converter. Hence, to determine the power characteristics of the ML-DAB becomes exceedingly difficult, especially in the case of a general n-L configuration.

In fact, owing to the tiny dwell time of Q2L modulation, the introduction of multilevel output has minimal impact on the power characteristics of the ML-DAB. Consequently, to analyze the power characteristics of the ML-DAB, the Q2L waveform of half-bridge A output voltage (u_{A}) can be decomposed into three components: the dc component ($u_{\mathrm{A,dc}}$), the square component ($u_{\mathrm{A,square}}$), and the Q2L component ($u_{\mathrm{A,q2l}}$), as depicted in Fig. 4.

Without loss of generality, assuming that $t_0 = 0$ for simplicity, the expression of u_{A} can be represented as follows:

$$\begin{aligned} u_{\mathrm{A}} &= u_{\mathrm{A},dc} + u_{\mathrm{A,square}} + u_{\mathrm{A},q2l} \\ &= \frac{V_1}{2} + V_1 u_s(t) + E u_\delta(t, \Delta T_{i\mathrm{A}}). \end{aligned} \tag{3}$$

In (3), $u_{\mathrm{s}}(t)$ represents the per-unit two-level square waveform with a magnitude of 0.5, as illustrated in Fig. 5. Additionally, $u_\delta(t, \Delta T_i)$ is the per-unit waveform resulting from Q2L modulation, as shown in Fig. 6.

With a similar decomposition of u_{A} and consideration of phase-shifting ratios, $u_{\mathrm{B}}, u_{\mathrm{a}}, u_{\mathrm{b}}$ can also be expressed as follows:

$$\begin{aligned} u_{\mathrm{B}} &= \frac{V_1}{2} + V_1 \cdot u_s(t - \frac{T}{2} - D_1 T) \\ &\quad + E \cdot u_\delta\left(t - \frac{T}{2} - D_1 T, \Delta T_{i\mathrm{B}}\right) \\ u_a &= \frac{V_2}{2} + V_2 \cdot u_s\left(t - D_0 T\right) \\ u_b &= \frac{V_2}{2} + V_2 \cdot u_s\left(t - D_0 T - \frac{T}{2} - D_2 T\right). \end{aligned} \tag{4}$$

Thus, by integrating Q2L modulation, MPS control, and the aforementioned definitions and decompositions, the equivalent circuit of the ML-DAB can be derived, as illustrated in Fig. 7.

$$\begin{cases} \sum_{i=1}^{\frac{n-2}{2}} i \cdot \Delta T_{ij} + \sum_{i=\frac{3n-4}{2}}^{2(n-2)} (2n-3-i)\Delta T_{ij} \\ = \sum_{i=\frac{n}{2}}^{n-2} (n-1-i)\Delta T_{ij} + \sum_{i=n-1}^{\frac{3(n-2)}{2}} (i-n+2)\Delta T_{ij}, & \begin{matrix}\mathrm{mod}(n,2)=0 \\ (j = \mathrm{A,B})\end{matrix} \\ \sum_{i=1}^{\frac{n-3}{2}} i \cdot \Delta T_{ij} + \sum_{i=\frac{3n-3}{2}}^{2(n-2)} (2n-3-i)\Delta T_{ij} \\ = \sum_{i=\frac{n+1}{2}}^{n-2} (n-1-i)\Delta T_{ij} + \sum_{i=n-1}^{\frac{3n-7}{2}} (i-n+2)\Delta T_{ij} & \begin{matrix}\mathrm{mod}(n,2)=1 \\ (j = \mathrm{A,B})\end{matrix} \end{cases}. \tag{2}$$

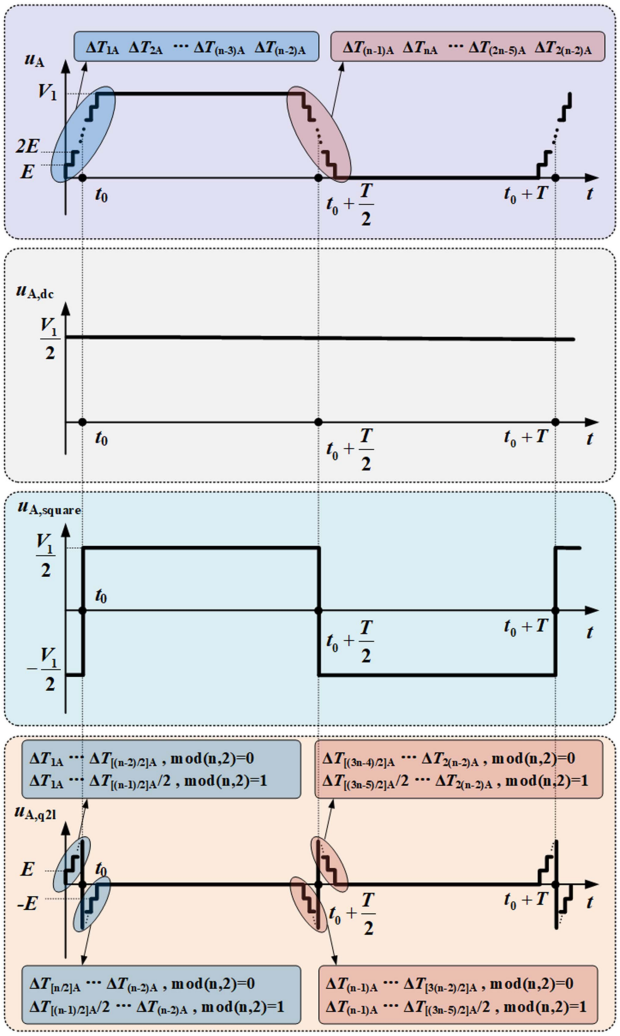

Fig. 4. Decomposition of multilevel half-ridge voltage u_{A}.

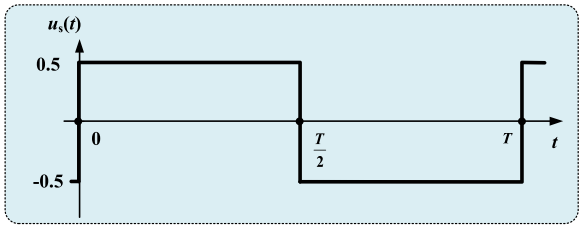

Fig. 5. Per-unit two-level square waveform $u_{\mathrm{s}}(t)$.

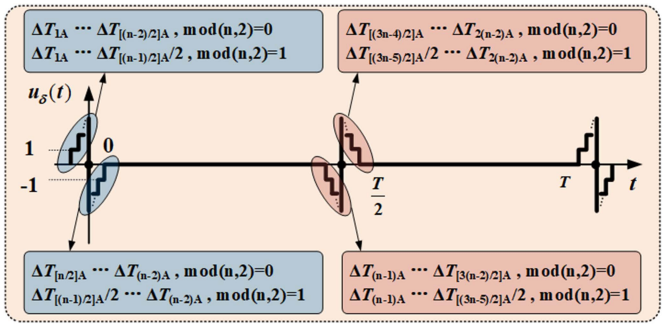

Fig. 6. Per-unit Q2L dwell time waveform $u_\delta(t)$.

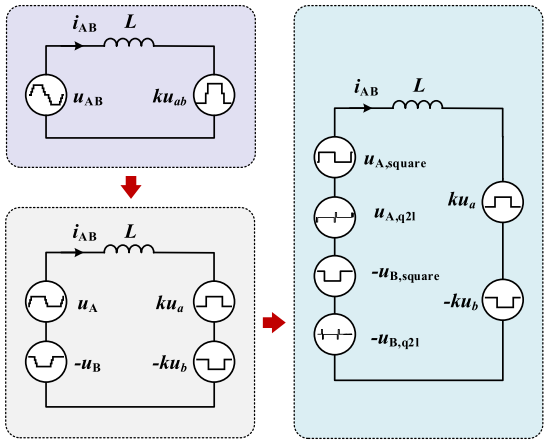

Fig. 7. Equivalent circuit of multilevel DAB.

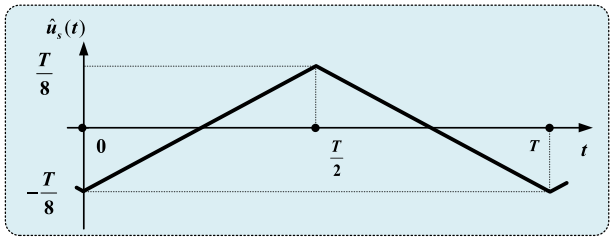

Fig. 8. Integral of $u_s(t)$: $\hat{u}_s(t)$.

Based on the equivalent circuit shown in Fig. 7, and with (3), (4) substituted, the differential equation of the leakage inductor current can be expressed as follows:

$$\begin{aligned} L_1\frac{di_{L_1}}{dt} &= u_{\mathrm{A}} - u_{\mathrm{B}} - k(u_a - u_b) \\ &= V_1 u_s(t) + E u_\delta\left(t, \Delta T_{i\mathrm{A}}\right) \\ &\quad - V_1 u_s\left(t - \frac{T}{2} - D_1 T\right) \\ &\quad - E u_\delta\left(t - \frac{T}{2} - D_1 T, \Delta T_{i\mathrm{B}}\right) \\ &\quad - kV_2\left(u_s(t - D_0 T)\right. \\ &\quad \left. - u_s\left(t - D_0 T - \frac{T}{2} - D_2 T\right)\right). \end{aligned} \tag{5}$$

For sake of simplicity, let the integral of $u_s(t), u_\delta(t, \Delta T_i)$ be denoted by $\hat{u}_s(t), \hat{u}_\delta(t, \Delta T_i)$, which varies periodically. Furthermore, it is evident that the offset of $\hat{u}_s(t), \hat{u}_\delta(t, \Delta T_i)$ is nullified due to the subtraction between the A and B bridge components. Hence, let us assume that $u_s(0) = -T/8$ for simplicity, and the specific magnitude and waveform of $\hat{u}_s(t)$ are shown in Fig. 8.

The leakage inductor current can be derived by solving (5), yielding the following expression:

$$i_{\mathrm{AB}}(t) = \left\{ \frac{1}{L_1} \begin{pmatrix} V_1\left[\hat{u}_s(t) - \hat{u}_s(t - \frac{T}{2} - D_1 T)\right] \\ -kV_2\left[\hat{u}_s(t - D_0 T)\right. \\ \left. -\hat{u}_s\left(t - D_0 T - \frac{T}{2} - D_2 T\right)\right] \end{pmatrix} \right\}$$

$$+\left\{\frac{E}{L_1}\left[\hat{u}_\delta\left(t,\Delta T_{i\mathrm{A}}\right)\right.\right.$$
$$\left.\left.-\hat{u}_\delta\left(t-\frac{T}{2}-D_1T,\Delta T_{i\mathrm{B}}\right)\right]\right\}$$
$$=\left\{\bar{i}_{L_1}\right\}+\left\{\tilde{i}_{L_1}\right\}. \tag{6}$$

Among (6), $\{\bar{i}_{L_1}\}$ represents the leakage inductor current component generated by the square component of voltage, $u_{\mathrm{AB,square}}$. Thus, $\{\bar{i}_{L_1}\}$ is not influenced by the dwell time of Q2L modulation and remains independent of $\Delta T_{i\mathrm{A/B}}$. Conversely, $\{\tilde{i}_{L_1}\}$ is the current component associated with Q2L modulation, and its magnitude is directly influenced by $\Delta T_{i\mathrm{A/B}}$. Considering the expression of $\{\tilde{i}_{L_1}\}$ and definition of $\hat{u}_\delta(t)$, the maximum of $\{\tilde{i}_{L_1}\}$ can be expressed as

$$\left\{\tilde{i}_{L_1}\right\}_{\max}=\begin{cases}\frac{E\Delta T_{\max}}{2L_1}n(n-2), & \mathrm{mod}(n,2)=0\\ \frac{E\Delta T_{\max}}{2L_1}(n-1)(n-2), & \mathrm{mod}(n,2)=1\end{cases}. \tag{7}$$

From (7), it can be seen that the maximum of $\{\tilde{i}_{L_1}\}$ is associated with the value of $\Delta T_{\max}$ and the number of voltage levels n, which is consistent with the above analysis. Moreover, to further elucidate and quantify the impact of the dwell time of Q2L modulation on the operation of ML-DAB, the equivalent phase-shifting ratio of 2L modulation to induce the same change in current can be deduced. Hence, to determine if the influence of dwell time on MPS control can be neglected, the maximum equivalent phase-shifting ratio $D_{\mathrm{eq,max}}$ can be obtained as follows:

$$\frac{(n-1)E}{L_1}D_{eq,\max}T=\frac{n(n-2)E}{2L_1}\Delta T_{\max}$$
$$D_{eq,\max}=\frac{n(n-2)}{2(n-1)}\frac{\Delta T_{\max}}{T}. \tag{8}$$

And a quantitative limit of $D_{\mathrm{eq,max}}$, D^*_{eq}, can be determined first, for example, 0.01, which is ignorable in practical implementation. And then the condition for neglecting the Q2L is as follows:

$$D_{eq,\max}\le D^*_{eq}. \tag{9}$$

Furthermore, when the value of $\Delta T_{\max}$ or the number of voltage levels increases, the rising edge/falling edge of proposed Q2L modulation will take a sizable proportion of the switching cycle. In that case, the Q2L component cannot be ignored directly, and thus the power flow cannot be controlled only by the three phase-shifting ratios of MPS. So indeed, there exits a limit on the maximum value of $\Delta T_{\max}$ or number of voltage levels that can be used, which can be deduced as follows:

$$\Delta T_{\max}\frac{n(n-2)}{2(n-1)}\le D^*_{eq}T. \tag{10}$$

Actually, for the NPC multilevel converter, due to the increasing number of devices, the number of voltage levels is generally less than 5, even if the MPS method can be applied in a case of more voltage levels. For a practical example of $n=4$, $f=20\,\mathrm{kHz}$ ($T=50\,\mathrm{us}$), and $\Delta T_{\max}=100\,\mathrm{ns}$, the equivalent phase-shifting ratio can be calculated specifically as (11), which is a negligible value for practical application

$$D^*_{eq}=0.00267. \tag{11}$$

Based on (11), it can be inferred that the contribution of $\{\tilde{i}_L\}$ can be negligible practically due to the small value of ΔT. Hence, the presence of ΔT also exerts minimal influence on the inductor current, and consequently on power transferring. Therefore, $\{\bar{i}_L\}$ can effectively substitute i_{AB} to a certain extent for analyzing the power characteristics of the ML-DAB.

On the other hand, the multilevel voltage u_{AB} can also be decomposed into $\bar{u}_{\mathrm{AB}}$ and $\tilde{u}_{\mathrm{AB}}$, expressed as

$$\begin{aligned}u_{\mathrm{AB}}&=u_{\mathrm{A}}-u_{\mathrm{B}}\\&=u_{\mathrm{A,square}}+u_{\mathrm{A},q2l}-\left(u_{\mathrm{B,square}}+u_{\mathrm{B},q2l}\right)\\&=u_{\mathrm{AB,square}}+u_{\mathrm{AB},q2l}\\&=\bar{u}_{\mathrm{AB}}+\tilde{u}_{\mathrm{AB}}\end{aligned} \tag{12}$$

where $\tilde{u}_{\mathrm{AB}}$ is also negligible compared to $\bar{u}_{\mathrm{AB}}$ due to the Q2L modulation.

With the premise of (6) and (12), the power characteristics of the ML-DAB under Q2L modulation and MPS control can be calculated as follows:

$$\begin{aligned}P&=\frac{1}{T}\int_0^T u_{\mathrm{AB}}\cdot i_{L_1}dt\\&=\frac{1}{T}\int_0^T(\bar{u}_{\mathrm{AB}}+\tilde{u}_{\mathrm{AB}})(\bar{i}_{L_1}+\tilde{i}_{L_1})dt\\&=\left\{\frac{1}{T}\int_0^T\bar{u}_{\mathrm{AB}}\cdot\bar{i}_{L_1}dt\right\}\\&\quad+\left\{\frac{1}{T}\int_0^T\left(\bar{u}_{\mathrm{AB}}\cdot\tilde{i}_{L_1}+\tilde{u}_{\mathrm{AB}}\cdot\bar{i}_{L_1}+\tilde{u}_{\mathrm{AB}}\cdot\tilde{i}_{L_1}\right)dt\right\}\\&=\left\{\bar{P}\right\}+\left\{\tilde{P}\right\}\end{aligned} \tag{13}$$

where $\{\bar{P}\}$ represents the power flow generated by the square voltage waveform and remains unaffected by Q2L modulation. On the contrary, $\{\tilde{P}\}$ accounts for the power flow associated with $\Delta T_{i\mathrm{A/B}}$, which is significantly smaller than $\{\bar{P}\}$ due to $\tilde{u}_{\mathrm{AB}}\ll\bar{u}_{\mathrm{AB}}$ and $\tilde{i}_{\mathrm{AB}}\ll\bar{i}_{\mathrm{AB}}$. Hence, it is entirely feasible to utilize $\{\bar{P}\}$ to control the power flow of the ML-DAB, especially when (10) is satisfied. Moreover, even in cases requiring precise power control or (10) is hard to satisfied, for example, a larger $\Delta T_{\max}$ or more voltage levels, it can be easily compensated through the fine-tuning of D_0, D_1, D_2 with closed-loop control.

$$\bar{P}=-\frac{2kV_1V_2}{TL_1}\begin{bmatrix}\int_{D_1T}^{\frac{T}{2}}\hat{u}_s(t-D_0T)dt\\-\int_{D_1T}^{\frac{T}{2}}\hat{u}_s\left(t-D_0T-\frac{T}{2}-D_2T\right)dt\end{bmatrix}. \tag{14}$$

The universal expression of $\{\bar{P}\}$ can be represented by (14). It is worth noting that the expression of $\bar{P}$ shares the same form with the power flow of the conventional 2L-DAB under TPS control [25]. Hence, considering $\bar{P}$ as the power flow of the ML-DAB with MPS control can simplify power flow control to the same extent as a 2L-DAB. Additionally, the existence of closed-loop control can guarantee the requirement for accurate control in practical application.

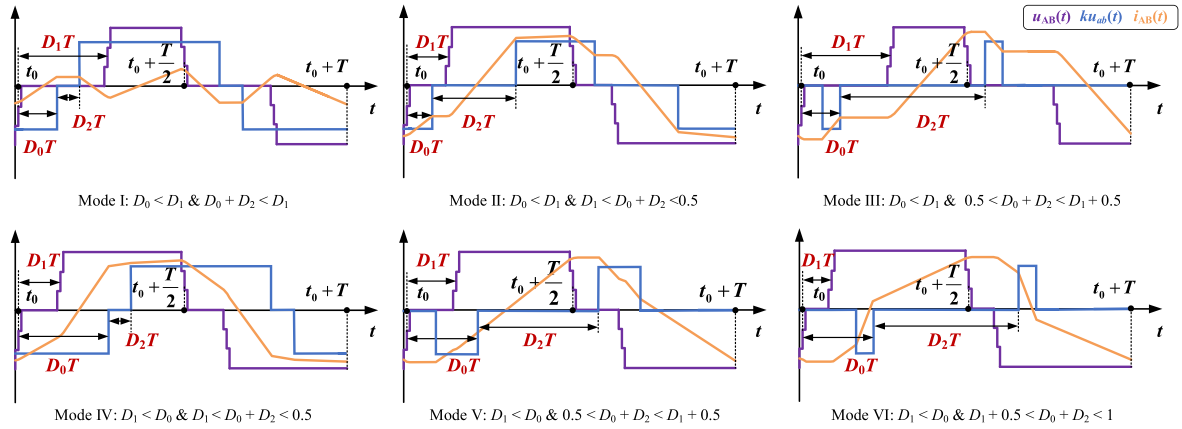

Fig. 9. Six operating modes of multilevel DAB under Q2L modulation and MPS control. (Taking 4L as an example).

TABLE II
DETAILED POWER CHARACTERISTICS OF SIX OPERATING MODES

Operating mode	Constraint	$P^*=f_i(D_0,D_1,D_2)$
Mode I	$D_0 < D_1$ & $D_0 + D_2 < D_1$	$f_1= 4(2D_0 - 4D_0D_1 + 2D_1^2 - D_1 + D_2 - 2D_1D_2)$
Mode II	$D_0 < D_1$ & $D_1 < D_0 + D_2 < 0.5$	$f_2= 4(D_2 - D_1 + 2D_0 - 2D_0^2 - 2D_2^2 + 2D_1D_2 - 4D_0D_2)$
Mode III	$D_0 < D_1$ & $0.5 < D_0 + D_2 < D_1 + 0.5$	$f_3= 4(\frac{1}{2} + 2D_1D_2 - D_1 - D_2)$
Mode IV	$D_1 < D_0$ & $D_1 < D_0 + D_2 < 0.5$	$f_4= 4(2D_1D_2 + 4D_0D_1 - 4D_0D_2 + 2D_0 + D_2 - D_1 - 4D_0^2 - 2D_1^2 - 2D_2^2)$
Mode V	$D_1 < D_0$ & $0.5 < D_0 + D_2 < D_1 + 0.5$	$f_5= 4(\frac{1}{2} + 2D_1D_2 + 4D_0D_1 - 2D_0^2 - 2D_1^2 - D_1 - D_2)$
Mode VI	$D_1 < D_0$ & $0.5 + D_1 < D_0 + D_2 < 1$	$f_6= 4(2D_2^2 + D_1 - 3D_2 - 2D_0 + 1 + 4D_0D_2 - 2D_1D_2)$

C. Power Modes of Multilevel DAB Under MPS Control

To get the unified power characteristics, assume that the power base value equals P_{base}, which is

$$P_{\text{base}} = \frac{kV_1V_2}{8fL_1}. \tag{15}$$

P_{base} represents the theoretical maximum power transfer of the ML-DAB, only when degrading into 2L condition. Hence, the per-unit power transfer can be expressed as follows:

$$P^* = \frac{\bar{P}}{P_{\text{base}}}. \tag{16}$$

Considering the symmetry of phase-shifting between primary and secondary sides, only the forward power transfer characteristics is focused sides in detail. For cases of backward power transfer, they can be realized by reserving the direction of outer phase shifting with same value. According to (7)–(11), $D_0T, D_1T, D_2T \gg \Delta T_{i\text{A/B}}$ can be easily satisfied in the practical operation of the ML-DAB. With this premise, it can be deduced that (14) has different detailed analytic expressions based on the relationship among D_0, D_1, and D_2. Thus, six different operating modes of the ML-DAB are accordingly defined. Fig. 9 illustrates the voltage and current waveforms of the ML-DAB under Q2L modulation and MPS control in these six operating modes, along with corresponding constraints of D_0, D_1, and D_2.

The specific analytic expressions of power transfer in different operating modes are presented in Table II, all of which are continuous with respect to D_0, D_1, and D_2. Therefore, the power range of different operating modes can be obtained by only searching for the maximum and minimum power transfer, which can be achieved through solving the optimization problems as follows:

$$\begin{aligned} &\max / \min P^* \\ &\text{s.t.} \begin{cases} P^* = f(D_0, D_1, D_2) \\ \text{Constraint of Mode i} \end{cases} \\ &(\text{i} = 1, 2, 3, 4, 5, 6). \end{aligned} \tag{17}$$

Fig. 10 illustrates the relationship between the power flow of the ML-DAB and the three phase-shifting ratios, along with the power range of each power mode, and the solution for the maximum power point. Moreover, to achieve a given power transfer P_{given}, the corresponding phase-shifting solution can be obtained by solving the optimization model below

$$\begin{aligned} &\min \quad (P^* - P_{\text{given}})^2 \\ &\text{s.t.} \begin{cases} P^* = f_i(D_0, D_1, D_2) \\ \text{Const. of Mode i} \end{cases} \\ &(i = 1, 2, 3, 4, 5, 6). \end{aligned} \tag{18}$$

After obtaining the solution from (18), due to the continuity of f_i, the real power flow can be precisely controlled to match

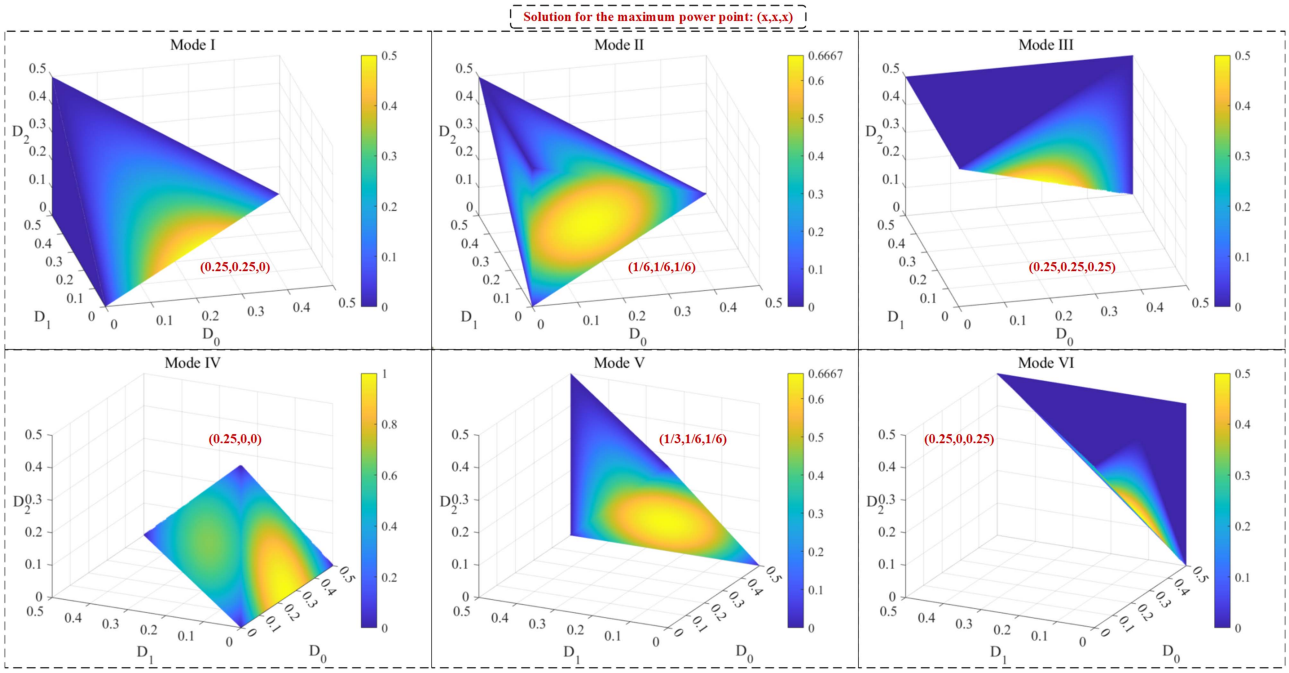

Fig. 10. Power range of six operating modes with D_0, D_1, and D_2.

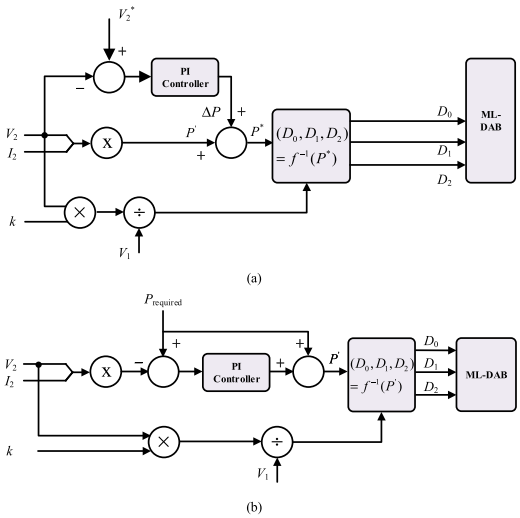

Fig. 11. Close-loop control of ML-DAB. (a) Output voltage control. (b) Output power control.

the given power flow by adjusting the phase-shifting ratios in a closed-loop manner to offset the slight impact of Q2L modulation, converter losses or any other factors that are difficult to calculate analytically, as illustrated in Fig. 11. Moreover, it should be noted that there could be multiple solutions for one certain P_{given} due to the existence of multiple power modes. And, thus, more flexibility is offered for the operating performance optimization control of ML-DAB, for example, the soft-switching performance optimization, which will be introduced in Section III.

III. Soft-Switching Optimization Control of Multilevel DAB

With the redundant degrees of freedom provided by the six power modes in (18), a criteria can be designed for selecting the most suitable power modes in operation for performance optimization, where some candidates include the ability to achieve soft-switching, the current stress, and ON-state loss. As the ML-DAB converter studied in this article is designed for high switching frequency, high power density applications, where the switching loss is the dominant factor in converter losses, the criteria for selecting the power mode in this section is, thus, on the soft-switching optimization control of ML-DAB converters, aiming to achieve full-range soft switching for switching loss reduction. Considering that the secondary side has the same topology and modulation as 2L DAB, it exhibits identical soft-switching performance to conventional 2L conditions. Therefore, this article mainly focuses on the soft-switching performance of the primary multilevel side. It should be noted that the proposed soft-switching optimization control method adapts for multilevel DAB converters of any levels. Different from most of the existing methods, the proposed optimization method do not require to conduct the detailed current expression of nL-DAB, but only utilizing the expression of equivalent current of conventional 2L-DAB, whose current expression is much easier to obtain.

A. Analysis of Soft-Switching Characteristics of ML-DAB

To achieve soft switching or not, the current at the moment when the devices switch ON/OFF plays a crucial role, as illustrated in Fig. 12. In case of $i_o > 0$ shown in Fig. 12(a), S_1 turns OFF

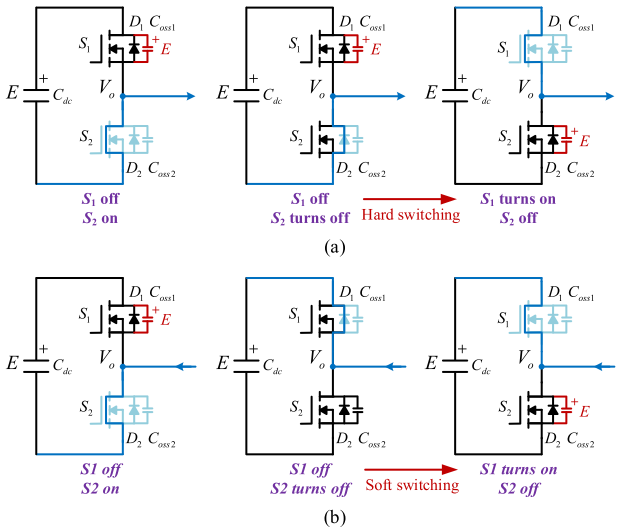

Fig. 12. Illustration of soft switching.

while bearing the voltage of E due to the conduction of D_2, resulting in hard switching. Consequently, the energy stored in the junction capacitor C_{oss1} is wasted due to the direct conduction of S_1. On the other hand, when $i_o < 0$, as in Fig. 12(b), the C_{oss1} is discharged to 0 before S_1 switches ON, and the energy stored in the capacitor is fed back to the dc bus. This occurs because the negative i_o can only flow through D_1 after the turning OFF process of S_2, enabling S_1 to achieve soft switching with ZVS ON.

Hence, to analyze the soft-switching characteristics of the ML-DAB, the inductor current, i_{AB}, should be studied first. As mentioned previously, the universal expression of the inductor current for ML-DAB with arbitrary levels can be obtained in (6). However, the Q2L component in (6), i.e., $\tilde{i}_{AB}$, makes it scarcely possible to obtain an analytic solution, especially when the level of the ML-DAB increases. In this article, an imaginary transient process from 2L to Q2L modulation is proposed, as shown in Fig. 13 (taking 4L-DAB as an example), which aids in analyzing the ML-DAB current with arbitrary levels.

In Fig. 13, the voltage and current waveforms under 2L modulation are depicted as red solid lines. At time t^*, the ML-DAB switches to Q2L modulation, illustrated as green solid lines, which sets all ΔT_{ij} to be ΔT initially and locates the $t_0{+}T$, $t_0{+}3T/2$ strictly in the middle of the rising/falling edge, as mentioned in Section II. The waveforms if maintaining 2L modulation are also shown as red dotted line after t^*, for clearer contrast. It is evident that the peak current remains unchanged during the transient process if the dark and light areas are equal, meaning the voltage impulses on the inductor are identical for 2L and Q2L modulation. This can be described as follows:

$$\begin{cases} \sum_{i=1}^{\frac{n-2}{2}} i\cdot\Delta T_{ij} \\ \quad=\sum_{i=\frac{n}{2}}^{n-2}(n-1-i)\Delta T_{ij} \\ \sum_{i=\frac{3n-4}{2}}^{2(n-2)}(2n-3-i)\Delta T_{ij} \\ \quad=\sum_{i=n-1}^{\frac{3(n-2)}{2}}(i-n+2)\Delta T_{ij} \end{cases}, \text{mod}(n,2)=0\ (j=\text{A},\text{B})$$

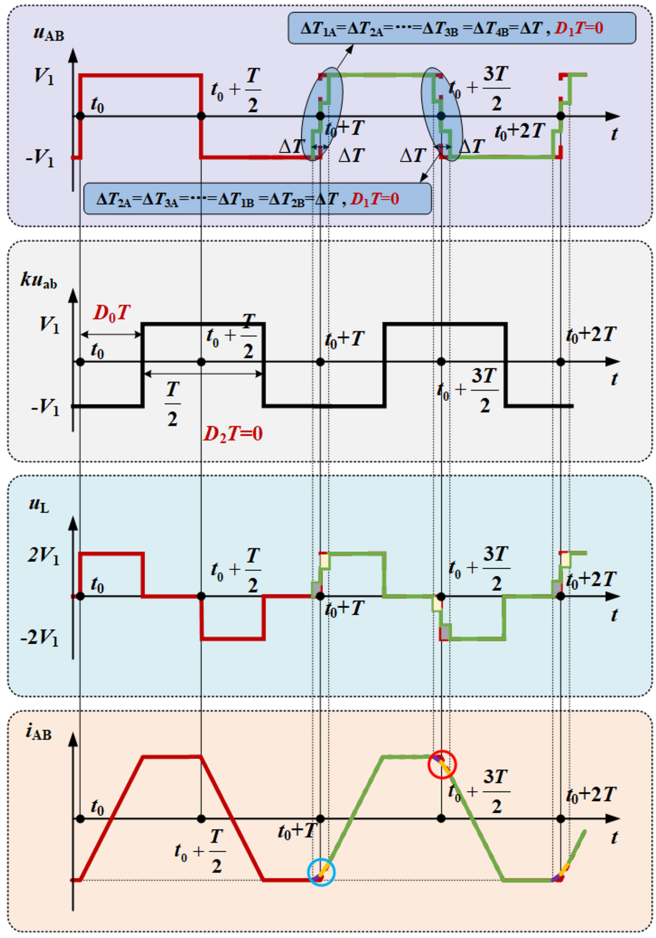

Fig. 13. Transient process from 2L to Q2L modulation of ML-DAB.

$$\begin{cases} \sum_{i=1}^{\frac{n-3}{2}} i\cdot\Delta T_{ij} \\ \quad=\sum_{i=\frac{n+1}{2}}^{n-2}(n-1-i)\Delta T_{ij} \\ \sum_{i=\frac{3n-3}{2}}^{2(n-2)}(2n-3-i)\Delta T_{ij} \\ \quad=\sum_{i=n-1}^{\frac{3n-7}{2}}(i-n+2)\Delta T_{ij} \end{cases}, \text{mod}(n,2)=1\ (j=\text{A},\text{B}). \tag{19}$$

It is important to note that with (19) satisfied, (2) is naturally fulfilled as well, ensuring that the voltage-second product of u_{AB} at each switching cycle is zero. And it should be highlighted that the adjustment of dwell time for capacitor voltage balancing control proposed in [24] has little impact on (19) averagely, considering the fluctuating adjusting process. Moreover, assuming that the 2L modulation of DAB has reached steady state before t^*, it remains steady for Q2L modulation just after t^* due to the invariance of half-cycle voltage impulses. Hence, the soft-switching characteristics of ML-DAB can be analyzed based on the current during $t_0+T\sim t_0+2T$ in Fig. 13.

To achieve soft switching of ML-DAB, the currents at the moment when the primary bridges switch, as circled in Fig. 13, should be entirely negative for the blue circle and entirely positive for the red circle. To ensure this, only the currents at the two ends of the circled intervals need to be bounded, due

to the monotonicity of the inductor current. Furthermore, it can be easily observed that the currents at the ends of the circled intervals are identical in the 2L and Q2L case.

Hence, the soft-switching characteristics of ML-DAB can be modeled with the inductor current of 2L DAB, $\bar{i}_L$, greatly reducing the complexity of optimization control for the ML-DAB and making it independent of the number of levels. The expression for $\bar{i}_L$, can be written as (20) shown at the bottom of this page, and it takes different forms depending on the relationship between D_0, D_1, and D_2, which has been studied extensively for the 2L DAB [25].

To illustrate more clearly, take the mode IV case shown in Fig. 9 as an example with $D_1 < D_0$ & $D_1 < D_0 + D_2 < 0.5$, and similar analysis can be conducted for the other power modes. The soft-switching constraint of ML-DAB can be described as (21), assuming $\Delta T_{iA} = \Delta T_{iB} = \Delta T_{\max}(i = 1, 2, \ldots, 2(n-2))$ for the toughest situation, which means that any $\Delta T \le \Delta T_{\max}$ in mode IV can achieve soft switching of ML-DAB with (21) satisfied

$$\begin{cases} \bar{i}_L\left(t_0 + T - \frac{n-2}{2}\Delta T_{\max}\right) < 0 \\ \bar{i}_L\left(t_0 + T + \frac{n-2}{2}\Delta T_{\max}\right) < 0 \\ \bar{i}_L\left(t_0 + T + D_1 T - \frac{n-2}{2}\Delta T_{\max}\right) < 0 \\ \bar{i}_L\left(t_0 + T + D_1 T + \frac{n-2}{2}\Delta T_{\max}\right) < 0 \\ \bar{i}_L\left(t_0 + \frac{3T}{2} - \frac{n-2}{2}\Delta T_{\max}\right) > 0 \\ \bar{i}_L\left(t_0 + \frac{3T}{2} + \frac{n-2}{2}\Delta T_{\max}\right) > 0 \\ \bar{i}_L\left(t_0 + \frac{3T}{2} + D_1 T - \frac{n-2}{2}\Delta T_{\max}\right) > 0 \\ \bar{i}_L\left(t_0 + \frac{3T}{2} + D_1 T + \frac{n-2}{2}\Delta T_{\max}\right) > 0. \end{cases} \tag{21}$$

Substituting the expression of 2L current $\bar{i}_L$ into (21), the soft-switching constraint can be expressed as (22). It can be observed that the soft-switching performance of the ML-DAB is influenced by three phase-shifting ratios, the matching degree of voltages at the primary and secondary sides, and the dwell time of Q2L modulation, in addition to the number of voltage levels. Importantly, the soft-switching characteristics exhibits a linear relationship with n, the number of voltage levels. This implies that the complexity of analysis does not increase with a higher number of voltage levels

$$\begin{cases} \frac{V_1}{L}\left(\frac{D_1 T}{2} - \frac{T}{4}\right) - \frac{kV_2}{L}\left(\frac{2D_0+D_2}{2}T - \frac{T}{4} - \frac{n-2}{2}\Delta T_{\max}\right) < 0 \\ \frac{V_1}{L}\left(\frac{D_1 T}{2} - \frac{T}{4} + \frac{n-2}{2}\Delta T_{\max}\right) \\ \quad - \frac{kV_2}{L}\left(\frac{2D_0-2D_1+D_2}{2}T - \frac{T}{4} - \frac{n-2}{2}\Delta T_{\max}\right) < 0 \\ \frac{V_1}{L}\left(\frac{T}{4} - \frac{D_1 T}{2}\right) - \frac{kV_2}{L}\left(\frac{T}{4} - \frac{2D_0+D_2}{2}T + \frac{n-2}{2}\Delta T_{\max}\right) > 0 \\ \frac{V_1}{L}\left(\frac{T}{4} - \frac{D_1 T}{2} - \frac{n-2}{2}\Delta T_{\max}\right) \\ \quad - \frac{kV_2}{L}\left(\frac{T}{4} + \frac{2D_1-2D_0-D_2}{2}T + \frac{n-2}{2}\Delta T_{\max}\right) > 0. \end{cases} \tag{22}$$

B. Full-Range Soft-Switching Optimization Control

With Q2L modulation and MPS control as the premise, the soft-switching characteristics of ML-DAB can be modeled similarly to the 2L case, as discussed previously. Just as the 2L DAB can achieve full-range soft switching by selecting appropriate power modes, it is also feasible for the ML-DAB. This can be achieved with the benefit of tiny ΔT of Q2L modulation, the six power modes under MPS control and the corresponding power characteristics given in Section II.

The power ranges in each power mode with the soft-switching constraint added can be determined through the optimization model, as shown in

$$\begin{aligned} &\max / \min P^* = f(D_0, D_1, D_2) \\ &\text{s.t.} \begin{cases} \text{Constraint of Mode i} \\ \text{Constraint of soft switching in Mode i} \end{cases} \end{aligned} \tag{23}$$

where the specific optimization model for mode IV is shown as follows:

$$\begin{aligned} &\max / \min P^* = f(D_0, D_1, D_2) \\ &\text{s.t.} \begin{cases} D_1 < D_0 \\ D_1 < D_0 + D_2 < 0.5 \\ \left(\frac{D_1}{2} - \frac{1}{4}\right) - \frac{kV_2}{V_1}\left(\frac{2D_0+D_2}{2} - \frac{1}{4} - \frac{n-2}{2}\frac{\Delta T_{\max}}{T}\right) < 0 \\ \left(\frac{D_1}{2} - \frac{1}{4} + \frac{n-2}{2}\frac{\Delta T_{\max}}{T}\right) \\ \quad - \frac{kV_2}{V_1}\left(\frac{2D_0-2D_1+D_2}{2} - \frac{1}{4} - \frac{n-2}{2}\frac{\Delta T_{\max}}{T}\right) < 0 \\ \left(\frac{1}{4} - \frac{D_1}{2}\right) - \frac{kV_2}{V_1}\left(\frac{1}{4} - \frac{2D_0+D_2}{2} + \frac{n-2}{2}\frac{\Delta T_{\max}}{T}\right) > 0 \\ \left(\frac{1}{4} - \frac{D_1}{2} - \frac{n-2}{2}\frac{\Delta T_{\max}}{T}\right) \\ \quad - \frac{kV_2}{V_1}\left(\frac{1}{4} + \frac{2D_1-2D_0-D_2}{2} + \frac{n-2}{2}\frac{\Delta T_{\max}}{T}\right) > 0. \end{cases} \end{aligned} \tag{24}$$

It can be observed that the model in (24) is identical to the 2L case if $\Delta T_{\max} = 0$. Considering that the 2L-DAB can achieve full-range soft switching with TPS, the major factor influencing the power range of soft switching for the ML-DAB is the ratio of $\Delta T_{\max}$ to T. Hence, benefiting from the tiny dwell time of Q2L modulation and the redundant freedom of MPS control, the ML-DAB can also achieve full-range soft switching, which can be facilitated by the proposed control strategy and implementation process shown in Fig. 14.

The detailed implementation processes are outlined as follows.

1) Determining the appropriate $\Delta T_{\max}$: To achieve full-range soft switching, the value of $\Delta T_{\max}$ is first required to be determined by the margin of MPS control and six power modes, which needs to make the optimization model (23) satisfied with maximum value of 1 and minimum value of 0, i.e., ensuring that the per-unit power flow $\bar{P}$ ranges from 0 to 1. This is associated with the given voltage matching of the primary and secondary

$$\bar{i}_L = \frac{1}{L_1}\left(V_1\left[\hat{u}_s(t) - \hat{u}_s(t - \frac{T}{2} - D_1 T)\right] - kV_2\left[\hat{u}_s(t - D_0 T) - \hat{u}_s(t - D_0 T - \frac{T}{2} - D_2 T)\right]\right). \tag{20}$$

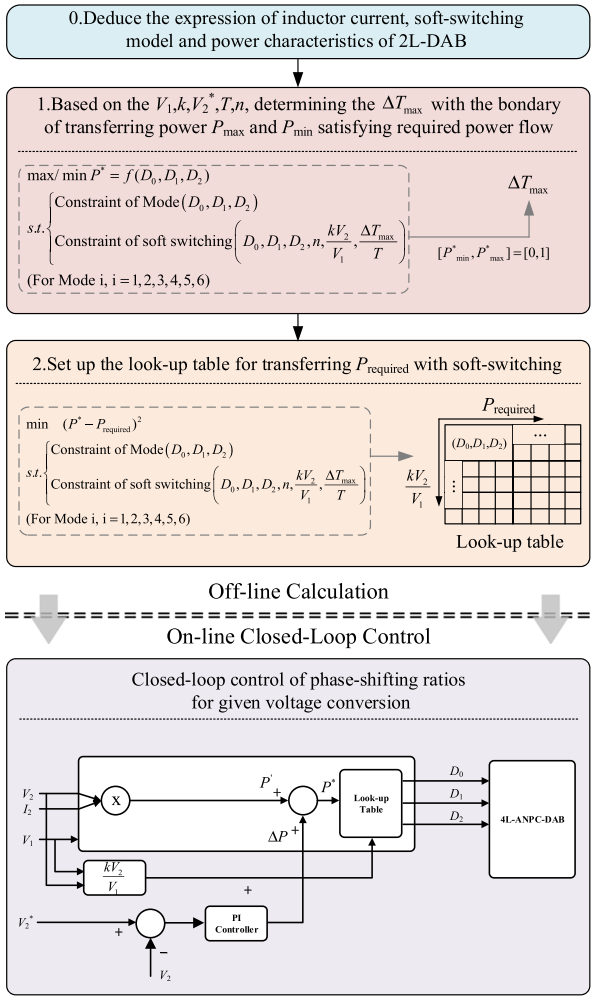

Fig. 14. Proposed full-range soft-switching optimization control of ML-DAB.

sides (kV_2/V_1), voltage levels (n), and switching period (T), and can be done by solving the (23) with certain $\Delta T_{\max}$ iteratively.

2) Setting up the look-up table for power flow: By solving the model in (25), which is exactly the model (18) along with the soft-switching constraint, the solution of $(D_0, D_1, D_2)^T$ required to transfer power of P_{required} in different voltage matching cases can be obtained and stored as a look-up table offline

$$\begin{aligned} &\min \quad (P^* - P_{\text{given}})^2 \\ &\text{s.t.} \begin{cases} P^* = f_i(D_0, D_1, D_2) \\ \text{Const. of Mode i} \end{cases} \\ &(i = 1, 2, 3, 4, 5, 6)\,. \end{aligned} \tag{25}$$

3) Closed-loop control with soft-switching optimization: To compensate the impact of Q2L modulation and nonideal parameters on the power flow of ML-DAB, a closed-loop control of voltage [or power, as shown in Fig. 11(b)] is adopted. The output of the PI controller provides the compensated power flow, which is based on the principle shown in Fig. 5. However, the three phase-shifting ratios are generated by the look-up table

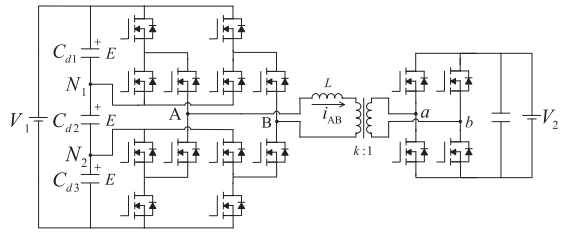

Fig. 15. Topology of 4L-ANPC-DAB.

established in 2), ensuring compliance with the optimization model and satisfying the requirement of soft switching. Hence, the adjustments from the PI controller do not affect the soft-switching performance.

As illustrated in Fig. 14, the control strategy primarily relies on the expressions derived for the 2L-DAB, such as the inductor current $\bar{i}_L$ shown in (20) and power flow $\bar{P}$ shown in Table II. With the proposed Q2L modulation and MPS control method, the multilevel DAB can operate in a way more like the conventional 2L-DAB, and the characteristics of 2L-DAB can be migrated to nL-DAB as the square-wave component $\bar{P}$. However, the migratation should be properly implemented and consider that if taking into account the little impact of the dwell time of Q2L modulation, which can be quantified as (10) and compensated by closed-loop control, as classified in Section II. In a word, the migration of 2L-DAB expressions significantly reduces the complexity of the ML-DAB and demonstrates good feasibility.

IV. Experimental Verifications and Comparison With the Existing Methods

To verify the effectiveness of the proposed Q2L modulation and MPS control for multilevel DAB, and validate the soft-switching optimization control strategy, a specific 4L-ANPC-topology shown in Fig. 15 has been studied for clearer clarification, including the detailed example of implementing process, experimental results with efficiency, and the theoretical comparison between the proposed method and existing method.

A. Detailed Example of Design and Implementation Process

The design and implementation process for 4L-ANPC-DAB is mainly same as the process shown in Fig. 14.

By combining the inductor current of 2L-DAB in (20) with the soft-switching requirements of multilevel DAB in (21), the detailed constraints of soft switching for 4L-ANPC-DAB ($n = 4$) can be derived. The detailed calculation example of soft-switching constraint of Mode I is attached as follows.

Substitute the inductor current expression (20) into the first inequation of (21), and we obtain (26) with $n = 4$, $t_0 = 0$ and the mode constraint of Mode I (D_0<D_1 & D_0+D_2<D_1)

$$\bar{i}_L(T - \Delta T_{\max}) < 0$$

$$\begin{pmatrix} V_1\left[\hat{u}_s(T - \Delta T_{\max}) - \hat{u}_s\left(\frac{T}{2} - \Delta T_{\max} - D_1 T\right)\right] \\ -kV_2\left[\hat{u}_s\left(T - \Delta T_{\max} - D_0 T\right)\right. \\ \left. -\hat{u}_s\left(\frac{T}{2} - \Delta T_{\max} - D_0 T - D_2 T\right)\right] \end{pmatrix} < 0$$

$$V_1\left(-\frac{T}{4}+\frac{D_1T}{2}+\Delta T_{\max}\right) - kV_2\left(-\frac{T}{4}+D_0T+\Delta T_{\max}+\frac{D_2T}{2}\right)<0. \quad (26)$$

Similar calculation process can be conducted for another 7 inequations of (21). And it should be noted that the first four expressions and the last four expressions in (21) have half-periodic symmetry with opposite polarity. Hence, the soft-switching constraint of Mode I can be summarized as follows:

$$\begin{cases} \left(-\frac{T}{4}+\frac{D_1T}{2}+\Delta T_{\max}\right) \\ \quad -\frac{kV_2}{V_1}\left(-\frac{T}{4}+D_0T+\Delta T_{\max}+\frac{D_2T}{2}\right)<0 \\ \left(-\frac{T}{4}+\frac{D_1T}{2}\right)-\frac{kV_2}{V_1}\left(-\frac{T}{4}+D_0T-\Delta T_{\max}+\frac{D_2T}{2}\right)<0 \\ \left(-\frac{T}{4}+\frac{D_1T}{2}\right) \\ \quad -\frac{kV_2}{V_1}\left(-\frac{T}{4}+D_1T-D_0T-\Delta T_{\max}-\frac{D_2T}{2}\right)<0 \\ \left(-\frac{T}{4}+\frac{D_1T}{2}\right) \\ \quad -\frac{kV_2}{V_1}\left(-\frac{T}{4}+D_1T-D_0T+\Delta T_{\max}-\frac{D_2T}{2}\right)<0. \end{cases} \quad (27)$$

Furthermore, the soft-switching constraints of other power modes can be obtained with the same way.

1) Determining the appropriate $\Delta T_{\max}$*:* It should be noted that the smaller the $\Delta T_{\max}$ is, the more similar with the 2L-DAB the characteristics of ML-DAB is, and thus, much easier to achieve full-range soft switching. Hence, the determining of the $\Delta T_{\max}$ can be illustrated as follows. With an initial $\Delta T_{\max}$ selected according to the practical switching frequency and switching speed of devices, the power ranges of each mode are calculated by (23). If the power range meets the requirement, the selected $\Delta T_{\max}$ is appropriate. Otherwise, the smaller one is needed to be verified iteratively.

The switching cycle of designed 4L-ANPC-DAB is 50 μs, and thus, the $\Delta T_{\max}$ selected is 1 μs. And then the according power ranges of each mode are calculated by (23) in consideration of the soft-switching constraints. And (28) gives the detailed example of calculation for Mode I, with kV_2/V_1 of 1, 4/3, and 1/3, to verify the soft-switching characteristics under different voltage matching degrees. Actually, it can achieve full-range soft switching under any voltage matching degrees with the freedom provided by six power modes.

$$\max/\min P^* = f_1(D_0,D_1,D_2)$$
$$\text{s.t.}\begin{cases} D_0<D_1 \\ D_0+D_2<D_1 \\ \left(-\frac{1}{4}+\frac{D_1}{2}+\frac{1}{50}\right)-\frac{kV_2}{V_1}\left(-\frac{1}{4}+D_0+\frac{1}{50}+\frac{D_2}{2}\right)<0 \\ \left(-\frac{1}{4}+\frac{D_1}{2}\right)-\frac{kV_2}{V_1}\left(-\frac{1}{4}+D_0-\frac{1}{50}+\frac{D_2}{2}\right)<0 \\ \left(-\frac{1}{4}+\frac{D_1}{2}\right)-\frac{kV_2}{V_1}\left(-\frac{1}{4}+D_1-D_0-\frac{1}{50}-\frac{D_2}{2}\right)<0 \\ \left(-\frac{1}{4}+\frac{D_1}{2}\right)-\frac{kV_2}{V_1}\left(-\frac{1}{4}+D_1-D_0+\frac{1}{50}-\frac{D_2}{2}\right)<0. \end{cases} \quad (28)$$

Finally, it can be calculated and proved that the $\Delta T_{\max}$ = 1 μs is appropriate for the designed 4L-ANPC-DAB.

2) Setting up the look-up table for power flow: With the model in (18), the operating points of transferring P_{given} under certain kV_2/V_1 can be solved and the feasible solution of D_0,D_1,D_2 can be stored as the look-up table. For the 4L-ANPC-DAB, a look-up table is established, as shown in Table III.

TABLE III
LOOK-UP TABLE FOR THE EXPERIMENTS OF 4L-ANPC-DAB

P_{given} \ kV_2/V_1	…	1/3	1	4/3
…	[D_0,D_1,D_2]	…	…	…
0.34	…	[0.17,0.22,0.37]		
…		…		
0.45			[0.02,0.13,0.3]	
…			…	
0.6		…		[0.28,0.16,0.22]
…				…
0.81			[0.2,0.05,0]	
…			…	

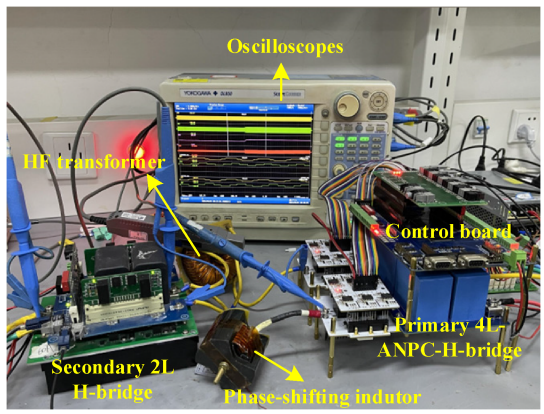

Fig. 16. 4L-ANPC-DAB prototype.

3) Closed-loop control with soft-switching optimization: With the look-up table shown in Table III, both the open-loop and closed-loop experiments are conducted for 4L-ANPC-DAB. The closed-loop control diagram adopted for 4L-ANPC-DAB is shown in Fig. 14, and a dynamic transition from V_o = 90 V to V_o = 120 V is set to verify the effect and performance of closed-loop control.

B. Experimental Results of 4L-ANPC-DAB

A 4L-ANPC-DAB experimental prototype is set up utilizing Wolfspeed SiC MOSFETS, CPM2-1700-0045, and CPM3-0900-0030A, as shown in Fig. 16. And the parameters of prototype are shown in Table IV.

Fig. 17 shows the experimental waveforms of 4L-DAB and 2L-DAB with identical phase-shifting ratios, D_0 = 0.2, D_1 = 0.05, D_2 = 0, which is in mode IV. The unified power flow in this case is 0.81, namely heavy load. First, it can be observed from Fig. 17 that with identical phase-shifting ratios, the power flow of 4L and 2L cases is same, which means that the Q2L modulation has little impact on the power flow of ML-DAB in heavy load. And they share same identical soft-switching performance.

Fig. 18 gives the comparison of 2L-DAB and 4L-DAB with light load, which is P^* = 0.45. Fig. 18(a) and (b) adopt identical

TABLE IV
PARAMETERS OF THE 4L-ANPC-DAB PROTOTYPE

Parameters	Values
Transformer turns ratio	1:1
Phase-shifting inductor	165 μH
Primary Voltage	90 V
Switching frequency	20 kHz
ΔT_{ij}	1 μs
P_{base} (V_{o}=90 V)	306.8 W
P_{base} (V_{o}=120 V)	409.1 W
P_{base} (V_{o}=30 V)	102.3 W

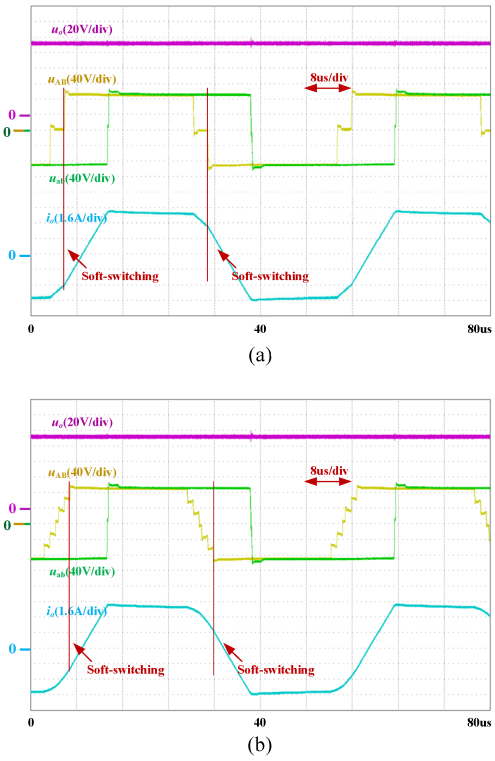

Fig. 17. Waveforms of 4L-DAB and 2L-DAB under P = 248 W (P^* = 0.81). (a) 2L-DAB (soft-switching). (b) 4L-DAB (soft-switching). (a) $D_0 = 0.2, D_1 = 0.05, D_2 = 0$, P = 248.1 W. (b) $D_0 = 0.2, D_1 = 0.05, D_2 = 0$, P = 248 W.

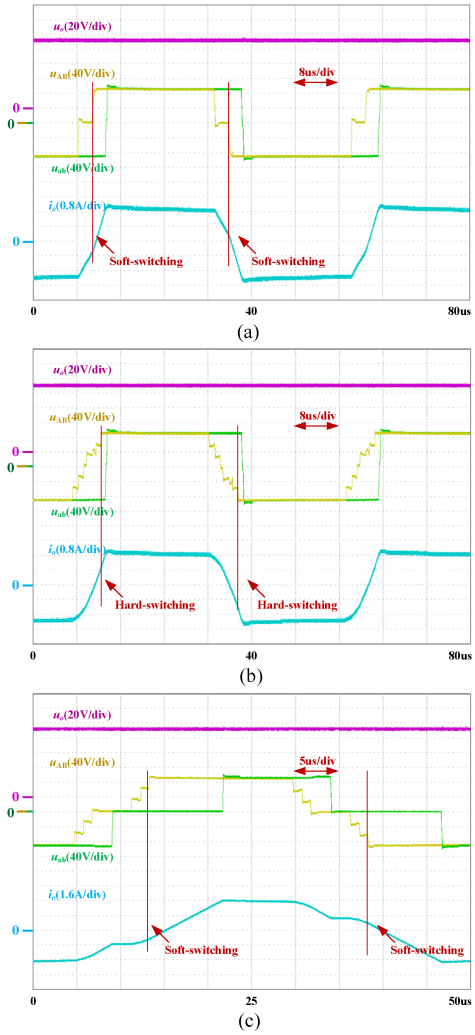

Fig. 18. Waveforms of 4L-DAB and 2L-DAB under (P^* = 0.45). (a) 2L-DAB, P = 137 W (soft-switching). (b) 4L-DAB, P = 131 W (hard-switching). (c) 4L-DAB, P = 137 W (soft-switching). (a) $D_0 = 0.1, D_1 = 0.05, D_2 = 0$. (b) $D_0 = 0.1, D_1 = 0.05, D_2 = 0$. (c) $D_0 = 0.02, D_1 = 0.13, D_2 = 0.3$.

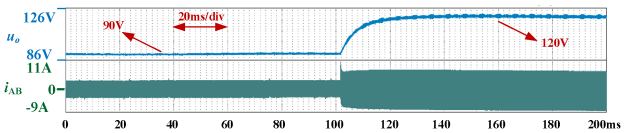

Fig. 19. Dynamic test results from $V_{\text{o}} = 90$ V to $V_{\text{o}} = 120$ V with load $R = 62\ \Omega$.

phase-shifting ratios of $D_0 = 0.1$, $D_1 = 0.05$, $D_2 = 0$, in mode IV. And it is clear to observe that the 2L-DAB can achieve soft-switching while the 4L-DAB loses the soft-switching. Hence, in light load, the impact of Q2L modulation cannot be ignored. Based on the soft-switching optimization control strategy in Section III, the 4L-DAB adopts $D_0 = 0.02$, $D_1 = 0.13$, $D_2 = 0.3$ of mode II, as shown in Fig. 18(c). Under thus circumstance, the 4L-DAB achieves soft-switching and transfers power flow identical with 2L-DAB in Fig. 18(a), which proves that the proposed closed-loop power flow control and soft-switching optimization corporate very well.

The experimental results of dynamic test for the proposed closed-loop control of 4L-DAB are given in Fig. 19. The transient process is with constant load $R = 62\ \Omega$, from $V_{\text{o}} = 90$ V to $V_{\text{o}} = 120$ V. The steady state of the dynamic test is set to be the state shown in Fig. 18(c) (Mode II). And Fig. 20 shows the steady-state results after the dynamic process, which is in mode V with $D_0 = 0.28$, $D_1 = 0.16$, $D_2 = 0.22$. It can be seen that the proposed control strategy maintains the achieving of soft-switching during closed-loop control process.

Fig. 21 shows the experimental results for $V_{\text{o}} < V_{\text{in}}$ ($V_{\text{o}} = 30$ V $= 1/3 V_{\text{in}}$), and it can be seen that the soft-switching can also be achieved at thus voltage-mismatched condition. However, it should be pointed that the operating state in Fig. 21 incurs high current stress while transferring low power flow, which can be optimized by further-optimized selection of operating point of ML-DAB.

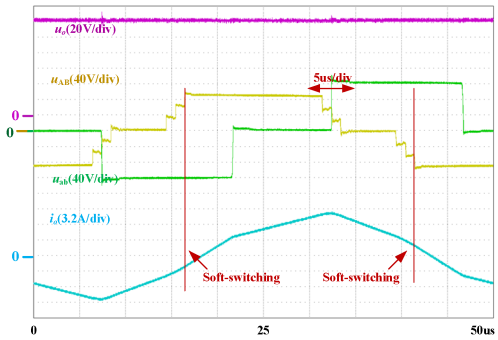

Fig. 20. Steady-state waveforms of above dynamic test for 4L-DAB. (V_o = 120 V with load $R = 62\ \Omega$, $D_0 = 0.28$,$D_1 = 0.16$,$D_2 = 0.22$, $P^* = 0.6$).

Fig. 21. Waveforms of 4L-DAB under $P^* = 0.34$. (V_o = 30 V with load R = 24.3 Ω, $D_0 = 0.17$,$D_1 = 0.22$,$D_2 = 0.37$).

TABLE V
EFFICIENCY RESULTS OF THE 4L-ANPC-DAB EXPERIMENTS

	P^*	$[D_0,D_1,D_2]$	Mode	V_2/V	P_{in}/W	P_{out}/W	η
1	0.81	[0.2,0.05,0]	2-Level	90	259.2	248.11	95.72%
2	0.81		IV		256.8	247.74	**96.47%**
3	0.45	[0.1,0.05,0]	2-Level		150.36	136.59	90.84%
4	0.45		IV	90	157.32	130.55	82.98%
5	0.45	[0.02,0.13,0.3]	II		149.34	137.1	**91.80%**
6	0.6	[0.28,0.16,0.22]	V	120	260.4	244.59	**93.93%**
7	0.34	[0.17,0.22,0.37]	III	30	41.4	33.67	**81.33%**

Table V summarizes the details of above experimental condition, together with the efficiency results. From the efficiency results, it can be seen that the proposed soft-switching performance optimization method based on Q2L modulation and MPS control works well in different condition and can improve the efficiency of multilevel DAB effectively.

C. Comparison With the Existing N-L Method

The comparison between proposed method and the conventional nL modulation method is given in Table VI, including the aspect of complexity, capacitor voltage balancing control, soft-switching range, advantages, disadvantages, and practical feasibility. The existing nL modulation and control method possesses more degrees of freedom, usually $2n$-1 variables for nL-DAB. The abundant variables take more flexibility for control, however, make the control of DAB much more complex meanwhile. And it is well-known that the TPS control provides enough degrees of freedom for 2L-DAB to control the power flow and optimize the operating performance, for example, the full-range soft-switching. Hence, it is possible to control the power flow and operating performance of nL-DAB, only using the three phase-shifting ratios of MPS method with the basis of Q2L modulation. And the proposed Q2L modulation and MPS control method can reduce the complexity of multilevel DAB and improve the feasibility of implementing multilevel DAB practically.

TABLE VI
COMPARISON BETWEEN PROPOSED METHOD AND CONVENTIONAL nL MODULATION

(For nL-DAB)	Proposed Q2L modulation and MPS control	Conventional nL modulation
Complexity(number of variables for DAB control)	3	2(n-1)
capacitor voltage balancing control	Decoupled with the DAB control	Coupled with the DAB control
Soft-switching range	Full-range	Full-range
Advantages	Sufficient degrees of freedom for control and easily implemented for arbitrary n-level DAB	More flexible degrees of freedom for multiobjective optimization
Disadvantages	Not enough degrees of freedom for multi-objective optimization	Complex to be implemented, especially for the DAB of more levels
Practical feasibility	High, especially for cases of 4L, 5L and nL DAB	moderate for the case of 3L-DAB

V. CONCLUSION

To improve the performance of multilevel DAB with feasible complexity, the Q2L modulation and MPS control suitable for arbitrary nL-DAB are proposed in this article. The characteristics of power flow, inductor current, and soft switching for ML-DAB are analyzed by migrating the 2L-DAB characteristics properly. And the control of ML-DAB converters is simplified as conventional 2L-DAB. Furthermore, an optimization control strategy to achieve full-range soft-switching is proposed. Experimental results of 4L-DAB prove that the proposed Q2L modulation, MPS control, and full-range soft-switching optimization strategy are of high effectiveness.

REFERENCES

[1] F. S. Al-Ismail, "DC microgrid planning, operation, and control: A comprehensive review," *IEEE Access*, vol. 9, pp. 36154–36172, 2021, doi: 10.1109/ACCESS.2021.3062840.

[2] L. Xu et al., "A review of DC shipboard microgrids—Part I: Power architectures, energy storage, and power converters," *IEEE Trans. Power Electron.*, vol. 37, no. 5, pp. 5155–5172, May 2022, doi: 10.1109/TPEL.2021.3128417.
[3] B. Zhao, Q. Song, W. Liu, and Y. Sun, "Overview of dual-active-bridge isolated bidirectional DC–DC converter for high-frequency-link power-conversion system," *IEEE Trans. Power Electron.*, vol. 29, no. 8, pp. 4091–4106, Aug. 2014, doi: 10.1109/TPEL.2013.2289913.
[4] G. Rødal and D. Peftitsis, "Design challenges of a SiC-based MVDC power supply for deep-sea applications," in *Proc. 10th Int. Conf. Power Electron. ECCE Asia*, 2019, pp. 2368–2375, doi: 10.23919/ICPE2019-ECCEAsia42246.2019.8797088.
[5] R. M. Burkart and J. W. Kolar, "Comparative $\eta-\rho-\sigma$ pareto optimization of Si and SiC multilevel dual-active-bridge topologies with wide input voltage range," *IEEE Trans. Power Electron.*, vol. 32, no. 7, pp. 5258–5270, Jul. 2017, doi: 10.1109/TPEL.2016.2614139.
[6] P. Liu, C. Chen, and S. Duan, "An optimized modulation strategy for the three-level DAB converter with five control degrees of freedom," *IEEE Trans. Ind. Electron.*, vol. 67, no. 1, pp. 254–264, Jan. 2020, doi: 10.1109/TIE.2019.2896209.
[7] Y. Ueuchi, N. Hoshi, and T. Ohno, "A transient characteristics improvement method in dual active bridge converter with multilevel inverter topology," in *Proc. Int. Power Electron. Conf. ECCE Asia*, 2022, pp. 1858–1864, doi: 10.23919/IPEC-Himeji2022-ECCE53331.2022.9806824.
[8] Q.-X. Guan, Y. Zhang, H.-B. Zhao, and Y. Kang, "Optimized switching strategy for ANPC–DAB converter through multiple zero states," *IEEE Trans. Power Electron.*, vol. 37, no. 3, pp. 2885–2898, Mar. 2022, doi: 10.1109/TPEL.2021.3118734.
[9] P. Liu, C. Chen, S. Duan, and W. Zhu, "Dual phase-shifted modulation strategy for the three-level dual active bridge DC–DC converter," *IEEE Trans. Ind. Electron.*, vol. 64, no. 10, pp. 7819–7830, Oct. 2017, doi: 10.1109/TIE.2017.2696488.
[10] L. Jin, B. Liu, and S. Duan, "ZVS soft switching operation range analysis of three-level dual-active bridge DC–DC converter under phase shift control strategy," *IEEE Trans. Ind. Appl.*, vol. 55, no. 2, pp. 1963–1972, Mar./Apr. 2019, doi: 10.1109/TIA.2018.2872121.
[11] Y. Xuan, X. Yang, W. Chen, T. Liu, and X. Hao, "A three-level dual-active-bridge converter with blocking capacitors for bidirectional electric vehicle charger," *IEEE Access*, vol. 7, pp. 173838–173847, 2019, doi: 10.1109/ACCESS.2019.2957022.
[12] Y. Wang, Y. Zhu, and H. Wen, "PSO-based current stress optimization for three-level dual active bridge DC-DC converters," in *Proc. Chin. Automat. Congr.*, 2020, pp. 4283–4287, doi: 10.1109/CAC51589.2020.9327782.
[13] Y. Wang et al., "Minimum-current-stress scheme of three-level dual-active-bridge DC–DC converters with the particle swarm optimization," *IEEE Trans. Transp. Electrific.*, vol. 7, no. 4, pp. 2067–2084, Dec. 2021, doi: 10.1109/TTE.2021.3073362.
[14] H. Higa and J. I. Itoh, "Derivation of operation mode for flying capacitor topology applied to three-level DAB converter," in *Proc. IEEE 2nd Int. Future Energy Electron. Conf.*, 2015, pp. 1–6, doi: 10.1109/IFEEC.2015.7361620.
[15] C. Song, Y. Yang, Z. Tang, and F. Blaabjerg, "Modulation of 2/3-level dual-active-bridge DC-DC converters for soft-switching and minimum current stress," in *Proc. IECON 46th Annu. Conf. IEEE Ind. Electron. Soc.*, 2020, pp. 2913–2918, doi: 10.1109/IECON43393.2020.9254624.
[16] J. Dong et al., "Hybrid Si + SiC neutral-point-clamped dual-active-bridge converter for high-voltage battery energy storage systems," in *Proc. IEEE 12th Energy Convers. Congr. Expo. - Asia*, 2021, pp. 632–637, doi: 10.1109/ECCE-Asia49820.2021.9479108.
[17] C. Song, Y. Yang, A. Sangwongwanich, and F. Blaabjerg, "Open-circuit fault analysis and fault-tolerant control for 2/3-level DAB converters," in *Proc. IEEE 12th Energy Convers. Congr. Expo. - Asia*, 2021, pp. 696–701, doi: 10.1109/ECCE-Asia49820.2021.9479285.
[18] Q. Gu, L. Yuan, S. Yi, J. Nie, and Z. Zhao, "Active selection of current commutation loop for hybrid three-level dual active bridge DC-DC converter with TPS control," in *Proc. IEEE 10th Int. Symp. Power Electron. Distrib. Gener. Syst.*, 2019, pp. 155–161, doi: 10.1109/PEDG.2019.8807680.
[19] Z. Guo and K. Sun, "Three-level bidirectional DC–DC converter with an auxiliary inductor in adaptive working mode for full-operation zero-voltage switching," *IEEE Trans. Power Electron.*, vol. 33, no. 10, pp. 8537–8552, Oct. 2018, doi: 10.1109/TPEL.2017.2780853.
[20] C. Song, A. Sangwongwanich, Y. Yang, Y. Pan, and F. Blaabjerg, "Analysis and optimal modulation for 2/3-level DAB converters to minimize current stress with five-level control," *IEEE Trans. Power Electron.*, vol. 38, no. 4, pp. 4596–4612, Apr. 2023, doi: 10.1109/TPEL.2023.3235938.
[21] C. Song, A. Sangwongwanich, Y. Yang, and F. Blaabjerg, "Optimal control of multilevel DAB converters for soft-switching and minimum current stress," *IEEE Trans. Power Electron.*, vol. 39, no. 5, pp. 5707–5720, May 2024, doi: 10.1109/TPEL.2024.3362051.
[22] F. Zhang, Y. Ren, X. Yang, W. Chen, and H. Wu, "Capacitor voltage balancing control for a novel 5-level dual active bridge converter," *IEEE Trans. Power Electron.*, vol. 37, no. 12, pp. 14738–14754, Dec. 2022, doi: 10.1109/TPEL.2022.3194960.
[23] A. Filba-Martinez, S. Busquets-Monge, and J. Bordonau, "Modulation and capacitor voltage balancing control of multilevel NPC dual active bridge DC–DC converters," *IEEE Trans. Ind. Electron.*, vol. 67, no. 4, pp. 2499–2510, Apr. 2020, doi: 10.1109/TIE.2019.2910035.
[24] J. Pang, K. Wang, Z. Zheng, T. Zheng, and Y. Li, "Quasi two-level operation and neutral-point voltage balance method for a four-level ANPC based dual active bridge DC-DC converter," in *Proc. IEEE Energy Convers. Congr. Expo.*, 2022, pp. 1–7, doi: 10.1109/ECCE50734.2022.9947940.
[25] J. Huang, Y. Wang, Z. Li, and W. Lei, "Unified triple-phase-shift control to minimize current stress and achieve full soft-switching of isolated bidirectional DC–DC converter," *IEEE Trans. Ind. Electron.*, vol. 63, no. 7, pp. 4169–4179, Jul. 2016.

Jupeng Pang (Student Member, IEEE) was born in Shandong, China, in 2000. He received the B.S. degree in electrical engineering in 2022 from the Department of Electrical Engineering, Tsinghua University, Beijing, China, where he is currently working toward the Ph.D. degree in electrical engineering.

His research interests include topology and control of multilevel converters, packaging, and application of wide band-gap semiconductor.

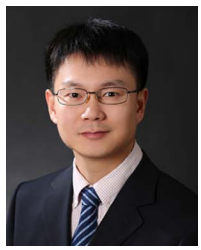

Kui Wang (Senior Member, IEEE) was born in Hubei, China, in 1984. He received the B.S. and Ph.D. degrees in electrical engineering from the Department of Electrical Engineering, Tsinghua University, Beijing, China, in 2006 and 2011, respectively.

From 2018 to 2019, he was a Visiting Scholar at the Center for Ultrawide-area Resilient Electric Energy Transmission Networks, University of Tennessee, Knoxville, TN, USA. He is currently an Associate Researcher with the Department of Electrical Engineering, Tsinghua University. His research interests include topology and control of multilevel converters, renewable energy generation, and wide band-gap semiconductor applications.

Dr. Wang was recognized as the distinguished reviewer for IEEE TRANSACTIONS ON POWER ELECTRONICS and IEEE TRANSACTIONS ON INDUSTRIAL ELECTRONICS, in 2022.

Mingzhe Wu (Member, IEEE) received the B.Sc. degree in electrical engineering from China University of Mining and Technology-Beijing, Beijing, China, in 2019, and the Ph.D. degree in energy systems from the University of Alberta, Edmonton, AB, Canada, in 2023.

From 2017 to 2019, he was a Research Assistant with the Department of Electrical Engineering, Tsinghua University, China, working on power system resilience and multilevel converters. He is currently a Lecturer with the Department of Electrical Engineering, China University of Mining and Technology-Beijing, Beijing, China. His current research interests include topology, modulation, and control of high-power converters.

Dr. Wu was the recipient of the Chinese Government Award for Outstanding Self-Financed Students Abroad in 2021.

Wei Zhou (Student Member, IEEE) received the B.S. degree in electrical engineering in 2022 from the Department of Electrical Engineering, Tsinghua University, Beijing, China, where she is currently working toward the M.S. degree in electrical engineering.

Her research interests include fault diagnosis of power converters, topology, and control of multilevel converters.

Zedong Zheng (Senior Member, IEEE) was born in born in Shandong, China, in 1980. He received the B.S. and Ph.D. degrees in electrical engineering from the Department of Electrical Engineering, Tsinghua University, Beijing, China, in 2003 and 2008, respectively.

He is currently an Associate Professor with Department of Electrical Engineering, Tsinghua University. His current research interests include power electronics converters and high performance motor control systems.

Yongdong Li (Senior Member, IEEE) was born in Hebei, China, in 1962. He received the B.S. degree from the Harbin Institute of Technology, Harbin, China, in 1982, and the M.S. and Ph.D. degrees from the Department of Electrical Engineering, Institute National Polytechnique de Toulouse, Toulouse, France, in 1984 and 1987, respectively, all in electrical engineering.

Since 1996, he has been a Professor with Department of Electrical Engineering, Tsinghua University, Beijing, China. He is the Lead Developer of the Power Electronics and Motor Control Laboratory, Tsinghua University. He was also an Invited Professor with the Institute National Polytechnique de Toulouse and the Dean with the School of Electrical Engineering, Xinjiang University, Urumchi, China. His current research interests include power electronics, machine control, and wind power generation.

Dr. Li is a Senior Member of the China Electro-Technique Society, the Vice Chairman of the China Power Electronics Society, and the Vice Chairman of the Electrical Automation Committee of China Automation Association.